EJN
European Journal of Neuroscience

European Journal of Neuroscience, Vol. 27, pp. 2587–2598, 2008 doi:10.1111/j.1460-9568.2008.06228.x

The medial nucleus of the trapezoid body in rat: spectral and temporal properties vary with anatomical location of the units

Sandra Tolnai,[1,2,3] Olga Hernandez,[1,2] Bernhard Englitz,[3,4] Rudolf Rübsamen[3] and Manuel S. Malmierca[1,2]
[1]Department of Cell Biology and Pathology, Faculty of Medicine, University of Salamanca, Salamanca, Spain
[2]Auditory Neurophysiology Unit, Laboratory for the Neurobiology of Hearing, Institute for Neuroscience of Castilla y Leon, University of Salamanca, Salamanca, Spain
[3]Institute of Biology II, University of Leipzig, Leipzig, Germany
[4]Max Planck Institute for Mathematics in the Sciences, Leipzig, Germany

Keywords: 3D reconstruction, auditory, *in vivo* electrophysiology, sinusoidally amplitude-modulated stimuli, superior olivary complex, temporal and spectral properties

Abstract

The medial nucleus of the trapezoid body (MNTB) is a distinct nucleus in the superior olivary complex that transforms excitatory input from the cochlear nucleus into a widespread inhibitory output to distinct auditory brainstem nuclei. Few studies have dealt with the response properties of MNTB neurons to sound stimulation using *in vivo* preparations. In order to have a better understanding of the functional significance of the MNTB in auditory processing we report the basic temporal and spectral response properties of its principal cells using single-unit extracellular recordings to acoustic stimulation with pure tones and amplitude-modulated stimuli in the rat. Ninety-seven per cent of units showed V-shaped frequency response areas. Rate level functions were mainly saturating (51%) or monotonic (45%) at high intensities. Post-stimulus time histograms typically were characterised as primary-like with notch (59%) or primary-like (33%). Units showed good phase-locking to sinusoidally amplitude-modulated signals with vector strength VS values up to 0.87. Modulation transfer functions had low-pass shapes at near-threshold levels, with cut-off frequencies ranging from 370 to 1270 Hz. Exploration of the relationship between the temporal and spectral properties and the location of the units in the MNTB yielded characteristic frequency (CF)-dependent response properties (latency, Q_{10} and cut-off frequency) following a medio-lateral gradient, and CF-independent response features (maximum firing rate) following a dorso-ventral gradient.

Introduction

The medial nucleus of the trapezoid body (MNTB) is one of the principal nuclei of the superior olivary complex that receives excitatory glutamatergic inputs from globular bushy cells in the cochlear nucleus (Harrison & Warr, 1962; Morest, 1968; Tolbert *et al.*, 1982; Grandes & Streit, 1989; Spirou *et al.*, 1990; Kuwabara *et al.*, 1991; Smith *et al.*, 1991; Malmierca, 2003). The MNTB in turn sends widespread projections to the lateral and medial superior olives and to the superior paraolivary nucleus (SPN) within the superior olivary complex, and to the ventral complex of the lateral lemniscus (Spangler *et al.*, 1985; Banks & Smith, 1992; Sommer *et al.*, 1993; Smith *et al.*, 1998). The MNTB neurons are glycinergic (Moore & Caspary, 1983; Wenthold *et al.*, 1987; Aoki *et al.*, 1988), transforming the excitatory input from globular bushy cells into an inhibitory output to the before-mentioned auditory brainstem nuclei.

The MNTB neurons receive their ascending input through large synaptic terminals, the calyces of Held (Held, 1893; Morest, 1968), which are specially suited for fast and reliable synaptic transmission (Chuhma & Ohmori, 1998; Taschenberger & von Gersdorff, 2000; Futai *et al.*, 2001), a key feature for processing interaural intensity differences in sound localisation (for review see Yin, 2002). The calyces of Held are the largest synaptic terminals in the mammalian brain, which makes the MNTB a unique structure suited as a model system for studying signal transmission at central synapses in brain slice preparations (Forsythe, 1994; Barnes-Davies & Forsythe, 1995; Borst *et al.*, 1995; for review see Schneggenburger & Forsythe, 2006). Detailed *in vivo* studies of MNTB neurons exemplifying their functional properties and responses to sound are less numerous, the earlier ones being done in cat (Guinan *et al.*, 1972a,b; Tsuchitani, 1997; Joris & Yin, 1998; Tollin & Yin, 2005). More recently, *in vivo* MNTB recordings were also obtained from rodents (rat: Sommer *et al.*, 1993; Paolini *et al.*, 2001; mouse: Kopp-Scheinpflug *et al.*, 2003a; gerbil: Kopp-Scheinpflug *et al.*, 2003b; rat: Kadner *et al.*, 2006), and these data might be more suited as reference for a functional interpretation of the many and diverse MNTB *in vitro* data. Still, the data in cats and rodents share many common features. They all show that MNTB neurons respond only to monaural stimuli presented to the contralateral ear (Sommer *et al.*, 1993; Joris & Yin, 1998; Kopp-Scheinpflug *et al.*, 2003a,b), and typically exhibit phasic-tonic responses and V-shaped frequency response areas (FRAs) to pure tone stimulation (Tsuchitani, 1997; Kopp-Scheinpflug *et al.*, 2003b).

The main goal of the present account was to present a detailed description of acoustically evoked response properties of MNTB neurons in rat using extracellular recordings. Both unmodulated

Correspondence: Dr M.S. Malmierca, [1]Department of Cell Biology and Pathology, as above.
E-mail: msm@usal.es

Received 13 November 2007, revised 29 February 2008, accepted 29 March 2008

pure tones and sinusoidally amplitude-modulated (SAM) stimuli were presented to characterise the units' frequency selectivity and the time course of responses. Furthermore, we made computer-assisted 3D reconstruction of the recording sites in the MNTB in order to analyse whether or not the units' response properties systematically vary as a function of their location within the MNTB.

Materials and methods

All experimental procedures were approved by the University of Salamanca Animal Care and Use Committee, and conformed to the guidelines of the EU directive 2003/65/CE and the Spanish RD 1201/2005. Extracellular single-unit activity was recorded from the MNTB of eight adult male rats (*Rattus norvegicus*; seven Long Evans pigmented, one Wistar albino strain), weighing between 208 and 264 g. Anaesthesia was induced with an intraperitoneal injection of urethane (1.5 g/kg) and maintained with supplementary doses (0.5 g/kg) to preserve an areflexive state. A tracheotomy was performed in order to assure adequate ventilation, and atropine sulphate was administered subcutaneously (0.05 mg/kg) to reduce bronchial secretions. Body temperature was monitored with a rectal probe and maintained at 38 ± 1 °C with a thermostatically controlled electrical blanket. The animal was placed in a stereotaxic frame in a sound-attenuated booth and fitted with hollow ear bars that accommodated the sound delivery system. A craniotomy was performed and the dura was reflected to allow electrode penetrations. The surface of the brain was irrigated regularly with saline to prevent desiccation.

Acoustic stimulation

Stimuli were synthesized by a System II workstation (Tucker-Davis Technologies) using custom software (SpikeSpain, kindly provided by B. Warren and E. Covey, University of Washington), and delivered through a closed field delivery system via two electrostatic speakers (TDT EC1) controlled by an electrostatic speaker driver (TDT ED1). The output of the system at each ear was calibrated *in situ* using a ¼″ condenser microphone (Brüel and Kjær 4136, Nærum, Denmark) and a DI-2200 spectrum analyser (Diagnostic Instruments, Livingston, Scotland, UK). The maximum output of the TDT system was flat from 0.3 to 5 kHz (≈100 ± 7 dB SPL) and from 5 to 40 kHz (90 ± 5 dB SPL). The highest frequency produced by this system was limited to 45 kHz. Second and third harmonic components in the signal were 40 dB or more below the level of the fundamental at the highest output level.

Data collection and analysis

A tungsten electrode (Merrill & Ainsworth, 1972) was placed over the exposed cerebellar cortex and moved along the dorsoventral axis using a piezoelectric microdrive (Burleigh 6000) that was advanced with a resolution of 1 μm by remote control from outside the booth. Single units were isolated presenting white noise and pure tones as searching stimuli. Action potentials were amplified (10 000×) with a Bioamp amplifier (TDT) and filtered (0.5–3 kHz, TDT DB4) before being processed in a spike discriminator (TDT SD1). The spike times were then stored on a computer.

FRAs of isolated single units were obtained by contralateral monaural stimulation with pure tones (75 ms, 5 ms rise/fall time, 4 Hz repetition rate) randomly varying in frequency (on a logarithmic scale) and attenuation. Each frequency/attenuation combination was presented 10 times. FRA borders were defined by determining the sound pressure levels at which firing rate significantly differed from spontaneous rate (Wilcoxon rank sum test, $P < 0.05$). The threshold was then identified as the lowest intensity occurring in the FRA border, i.e. as the lowest intensity eliciting a response. Characteristic frequency (CF) was defined as the response to a given sound frequency with the lowest threshold. Sharpness of tuning was measured by determining Q_n values, defined as the CF divided by the difference between the upper and lower frequencies of the FRA at '*n*' dB above threshold. Further, the 'square-root transform of bandwidth' ($root_n$) was calculated (Calford *et al.*, 1983). The $root_n$ is defined as the difference between the square-roots of the upper and lower frequencies of the FRA at '*n*' dB above threshold. The steepness of FRA borders was determined by calculating the inverse slope (IS) for the low- and high-frequency edges. IS is defined as IS = $\Delta f/\Delta$dB, where Δf is expressed in octaves and ΔdB is measured by fitting a regression line through each border of the FRA between 5 and 35 dB above threshold (Sutter, 2000). Negative values indicate slopes toward lower frequencies at higher intensities. For comparison IS values are expressed as octaves/40 dB (Sutter, 2000; Hernandez *et al.*, 2005). Rate level functions (RLFs) were obtained by presenting 10 repetitions of pure tones (75 ms duration, 5 ms rise/fall time) at the units' CFs at different intensities presented randomly. The dynamic range was defined as the range of intensities at which firing rates both differed significantly from spontaneous and maximum rates (Wilcoxon rank sum test, $P < 0.05$). Post-stimulus time histogram (PSTH) data were recorded in response to 50 repetitions of tone bursts at the units' CFs (duration, 100 ms; delay, 10 ms; repetition rate, 5 Hz) at 0 dB attenuation.

Carrier frequency of SAM stimuli was set at unit's CF (200 ms duration, 5 rise/fall time, repetition rate 4 Hz). Modulation frequencies were varied randomly between 20 and 2000 Hz (logarithmic scaling, maximum f_{AM} = 1/2 CF) and presented to the contralateral ear (20 repetitions). Stimulus levels were typically 10 or 20 dB above threshold. In some units additional stimulus levels were tested. Modulation depth (m) of SAM stimuli was usually 100%, but in some units also 75, 50 and 25% modulation depths were tested.

The vector strength (VS) was calculated for responses to SAM stimulations for each modulation frequency and for responses to pure tones, according to Goldberg & Brown (1969)

$$\mathrm{VS} = \sqrt{\left(\sum_{\text{spikes}} \cos(\alpha)\right)^2 + \left(\sum_{\text{spikes}} \sin(\alpha)\right)^2} \Big/ n,$$

where the sum runs over all spikes, α denotes the phase of each spike with respect to the period of the stimulus and n is the total number of spikes. The first 20 ms of the responses were excluded from the analysis to eliminate effects of the onset peak. The statistical significance of the VS was evaluated using the Rayleigh test ($P = 0.05$).

Modulation gain was calculated for the responses to SAM stimuli with $m < 100\%$ by:

$$\mathrm{gain} = 20 \times \log\left(\frac{2\mathrm{VS}}{\mathrm{m}}\right)$$

Units' response latencies were measured with a modified reverse correlation method, termed the periodic cross-correlation method using responses to SAM stimuli (100% modulated). First, the cross-correlation between the SAM envelope and the resulting PSTH was

computed for each f_{AM} tested. Maxima in each cross-correlation correspond to latencies of best agreement between stimulus envelope and response PSTH. Because the stimuli are periodic, the cross-correlations are also periodic. To select the maximum correspondence to the actual latency, multiple cross-correlations for different values of f_{AM} were superimposed. The latency at which most maxima aligned was taken to be the actual latency. More precisely, a smoothed histogram of the maxima's positions was constructed by convolving each maximum's position with a Gaussian kernel (SD 0.3 ms) and adding the resulting vectors. The maximum of the resulting vector is positioned at the correct latency. Only values of $f_{AMS} \geq 500$ Hz were used, as in this range the correlation maxima overlapped precisely (about 0.2 ms).

Data analysis was performed using custom-written software in MATLAB 7.1 (The Mathworks, Nattick, MA, USA). Statistical analysis was performed using SIGMASTAT/sigmaplot (SPSS Science, Chicago, IL, USA). Unless stated otherwise, data are expressed as means and standard deviations, if normally distributed; otherwise medians and 25th and 75th percentiles are used.

Verification of recording sites

At the end of each recording track, recording sites were verified by placing electrolytic lesions (5 μA, 5 s). The animal was killed with a lethal dose of sodium pentobarbital (Nembutal; 60 mg/kg in saline, intraperitoneal) at the end of the recording session, and perfused transcardially with Ringer's solution followed by fixative (1% paraformaldehyde and 1% glutaraldehyde in 0.1 M phosphate buffer, pH 7.4). After 2–4 days of post-fixation, the brain was blocked in a single piece that contained the brainstem and immersed in a 30% sucrose solution for two to three additional days until it sunk. The tissue was cut in serial sections in the transverse plane (40-μm thick) using a freezing microtome. The sections were mounted on slides, stained with Cresyl violet and examined under the light microscope.

We reconstructed 26 electrode tracks with electrolytic lesions from six cases using Neurolucida (Microbrightfield). The locations of the units were visualized in 3D after connecting lesions made in selected recordings with known CFs. We calculated the relative position of each unit along the tracks; thereby we obtained information on the relationship between the CFs recorded at different locations and the tonotopic arrangement of the units within the MNTB. These data served as the basis for the plots shown in Fig. 8.

Results

The present results are based on 70 well-isolated single units from the MNTB. Units were identified as being MNTB units by the occurrence of prepotentials in their action potential waveforms (Fig. 1B, inset), which allowed the distinction from trapezoid fibres (Guinan & Li, 1990; Smith *et al.*, 1998; Kopp-Scheinpflug *et al.*, 2003b), and by the location of the electrolytic lesions and subsequent reconstruction of recording sites within the MNTB in 3D (see Fig. 8). In the following, we will first describe the physiological properties of MNTB units inferred from their response properties to pure tone stimulation and SAM stimulation. Then, we will detail the relationship between the respective response properties and the recording sites within the MNTB.

Responses to unmodulated pure tone stimulation

Spectral properties of MNTB units were analysed by means of FRAs. FRAs were acquired from 64 units. For six units only part of the FRA could be obtained. The CFs ranged from 0.9 to 40 kHz, and had minimum thresholds at CF from −2 to 71 dB SPL (Fig. 1B). The sample of units covered mainly the high-frequency range of the behaviourally tested auditory range for the hooded rat (Heffner *et al.*, 1994); ∼92% of units (59/64) had CFs > 6 kHz (Fig. 1B). This high-frequency bias is in accord with previous data from Sommer *et al.* (1993), and points to the fact that the MNTB provides the major contralateral input to the lateral superior olive, which itself is predominantly tuned to higher frequencies (for detailed discussion see Tollin & Yin, 2005).

In a first approach FRAs were classified by eye. The majority of units (97%, 62/64) had V-shaped FRAs (Fig. 1A), i.e. the shape bore the typical characteristics of auditory nerve fibres (Kiang *et al.*, 1967, 1976; Sachs & Abbas, 1974; Schmiedt, 1989; el Barbary, 1991b), a clear identifiable CF and a widening of the frequency response range to higher intensities (Fig. 1A,a). About half of the units showing V-shaped FRAs (47%, 29/62) featured a distinct low-frequency tail (Fig. 1A,b–d). We also quantified the shape of the FRAs by calculating the ISs (Sutter, 2000; Hernandez *et al.*, 2005) for the low- and high-frequency borders (IS_L and IS_U, respectively) of the FRA expressed as octaves/40 dB. Figure 1C shows a scatter plot in which each point represents the coordinates for the IS_U on the abscissa and IS_L on the ordinate. Most units had positive values for IS_U and negative values for IS_L, which confirms that most units are of asymmetric V-shaped type with or without a low-frequency tail.

In six units, the FRAs showed clear inhibitory sidebands at the high-frequency side (Fig. 1A,c); inhibitory sidebands to the low-frequency side were not observed. In principle, inhibitory sidebands cannot be observed by the use of single tone stimulation in units that lack spontaneous activity, as inhibition can only be assessed as a significant reduction of spontaneous rate. Another six units in our sample showed a decrease in firing rate at high levels at CF and were classified as non-monotonic V-shaped FRAs (Fig. 1A,d).

Only two units in our sample did not show a typical V-shaped FRA, they were broadly tuned and had shallow slopes on both the low- and high-frequency borders of the FRA.

Sharpness of tuning was quantified by determining: (i) Q_n values (Fig. 1D), as these metrics are the most commonly used measurement for describing the sharpness of FRAs; and additionally by (ii) square-root transforms of bandwidth ($root_n$), which do not vary with CF (Calford *et al.*, 1983; Fig. 1E). Units' Q_{10} and Q_{30} values increased with increasing CF (Fig. 1,D1 and D2; Spearman rank order correlation: 0.533 and 0.484, respectively, and $P < 0.001$). As expected, $root_{10}$ and $root_{30}$ values (Fig. 1,E1 and E2) were not correlated to CF ($P > 0.05$).

Temporal response types were classified from PSTHs in 54 units (Fig. 2) to tone burst stimulation at the units' CF at 20–70 dB above threshold, corresponding to 53–110 dB SPL. The majority of units (94%, 51/54) featured a phasic-tonic response pattern. Of those, 32 units were classified as primary-like notch response type (Fig. 2A), 18 units as primary-like response type (Fig. 2B) and one unit showed a phase-locked response (Fig. 2C). Three units lacked the phasic component and solely showed a sustained response pattern (Fig. 2D).

Maximum firing rates (maxR) were determined for 64 units. Mean maxR were calculated for the total duration of pure tone pulses, and were in the range of 100–560 Hz with the median at 325 Hz (25th and 75th percentiles: 230 and 390 Hz; Fig. 3A). The maximum onset rates of units' responses could be up to sixfold higher than maxR. Instantaneous rates during the onset peak varied between 320 and 1880 Hz (mean: 1140 Hz; SD: 335 Hz; Fig. 3A). MaxR and onset rates were independent of CF.

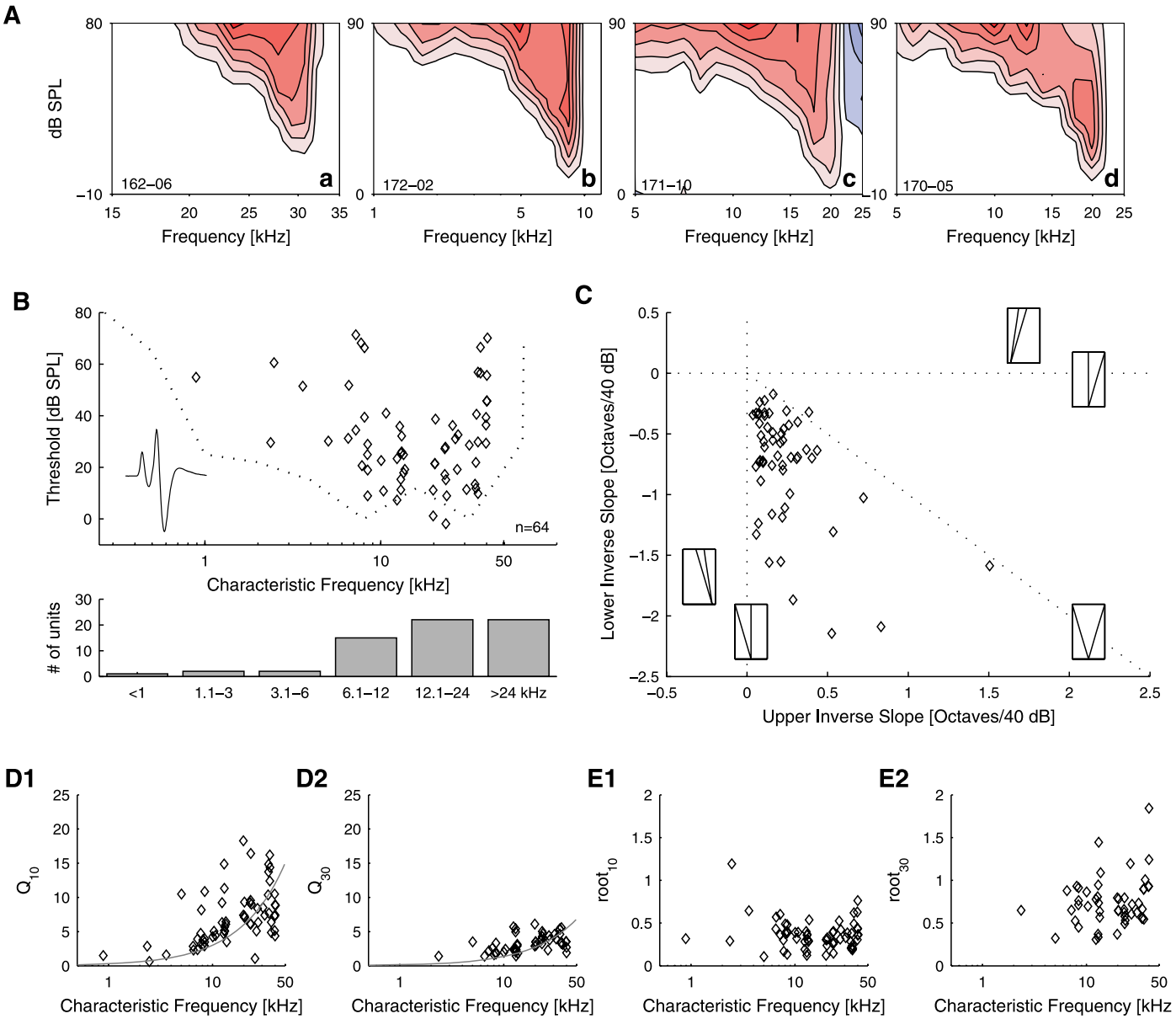

FIG. 1. Tuning properties of MNTB units. (A) V-shaped FRAs shown as contour plots of firing rate across frequencies and sound pressure levels. Firing rates are shown relative to spontaneous activity and normalised to the difference between maxR and spontaneous rate. Red areas indicate firing rates above spontaneous activity, blue areas firing rates below spontaneous activity. (a) V-shaped FRA (33/62 units). (b) V-shaped FRA with low-frequency tail (29/62 units). (c) FRA bordered by a high-frequency sideband (6/62 units). (d) Non-monotonic FRA (6/62 units), i.e. as sound intensity increases firing rate at CF decreases. (B) Thresholds and CFs. Thresholds of 64 single units at CF tones ranged between −2 and 71 dB SPL (top). The hooded rat's behavioural audiogram (dotted line; Heffner *et al.*, 1994) is included for comparison. The majority of units had CFs > 6 kHz (bottom). Inset in (B) shows the mean potential waveform of an MNTB unit recorded extracellularly. The waveform typically consists of the prepotential followed by the action potential. (C) Scatter plot with data points representing the coordinates of upper ISs of FRA borders on the abscissa and lower ISs of FRA borders on the ordinate. The diagonal dotted line denotes FRAs with symmetric borders. Vertical and horizontal dotted lines indicate boundaries of greatest asymmetry between lower and upper FRA borders (see respective sketches in the insets). (D and E) Sharpness of tuning displayed as Q_{10} and Q_{30} values (D1 and D2), and as square-root transforms of bandwidth at 10 and 30 dB above threshold ($root_{10}$, $root_{30}$; E1 and E2). While Q_n values increase with higher CF ($P < 0.001$, Spearman rank order correlation 0.533 and 0.484, respectively), $root_n$ do not show any dependence on CF ($P > 0.05$).

About two-thirds of units (44/64) showed their maxR at the highest sound level tested, corresponding to 84–110 dB SPL (median: 100, 25th and 75th percentiles: 97 and 110 dB SPL). The remaining 20 units had their maxR at lower levels (10–40 dB), corresponding to 58–98 dB SPL (median: 78, 25 and 75% percentiles: 67 and 81 dB SPL).

About three-quarters of the units (49/64) had their maxR at frequencies off CF (Fig. 3A, open triangles), typically at frequencies below CF (94%, 46/49). The median difference between CF and best frequency (stimulus frequency evoking the highest firing rate) was 0.24 octaves (25th and 75th percentiles: 0.15 and 0.67 octaves). In units where best frequency differed from CF, median firing rates at best frequency were 40 Hz (25th and 75th percentiles: 20 and 85 Hz) higher than at the corresponding level at CF.

Spontaneous activity of the units (Fig. 3A) varied between 0 and 133 Hz, with the median value at 18 Hz (25th and 75th percentiles: 3 and 48 Hz). More than half of the units (53%, 37/70) showed a

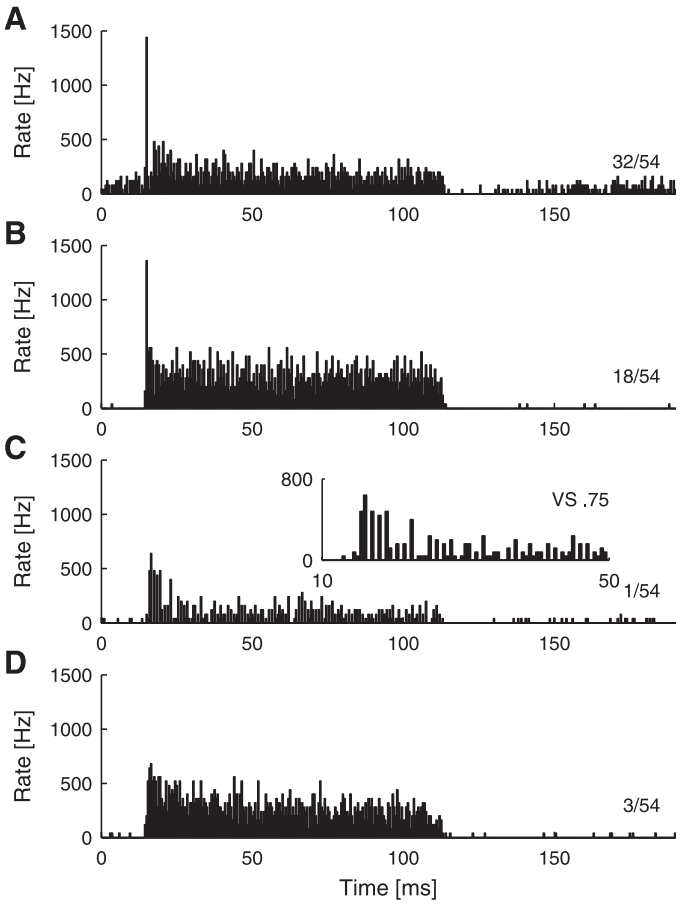

FIG. 2. PSTHs. PSTH of the (A) primary-like with notch and (B) primary-like response type. (C) Phase-locked response type. Unit's CF was 0.9 kHz. The inset gives an expanded view of the first 40 ms of the response. The vector strength (VS) of the response was 0.75. (D) Tonic response type. Data were recorded in response to 50 repetitions of tone bursts at the units' CFs (duration 100 ms, stimulus onset 10 ms). Bin width: 0.5 ms. CF and stimulus level of recording: (A) 12.4 kHz, 70 dB SPL; (B) 34.7, 70 dB SPL; (C) 0.9 kHz, 95 dB SPL; (D) 14.9 kHz, 80 dB SPL.

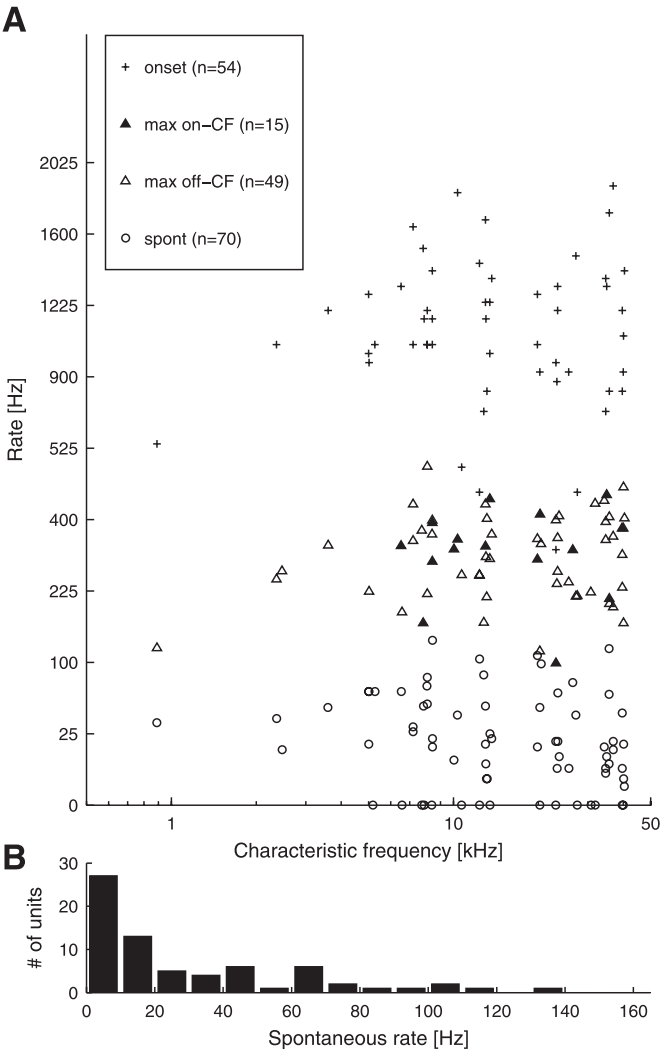

FIG. 3. Spontaneous and stimulus-evoked discharge activity. (A) Onset rates (+, peak instantaneous firing rate at response onset), maxR (open triangle and closed triangle, highest mean firing rate throughout FRA) and spontaneous rates (○) of units. MaxR could either occur at a unit's characteristic frequency (CF) (closed triangle) or off CF (open triangle). Rate is shown on a square-root scale. (B) More than half of the units had spontaneous rates <20 Hz.

spontaneous activity of <20 Hz, with 15/37 units not being spontaneously active at all (Fig. 3B). One-fifth of units (14/70) had very high spontaneous rates (>60 Hz). The bimodal distribution reported for spontaneous rates of auditory nerve fibres (Liberman, 1978; Schmiedt, 1989; el Barbary, 1991a) was not observed in the present data. Spontaneous rate was neither correlated to CF nor to maxR.

RLFs were obtained for 64 units (Fig. 4) by presenting tone bursts at the units' CF with systematic variations of the sound levels in 10-dB steps (tone duration: 75 ms; repetition interval: 250 ms; 10 repetitions). More than half of the units (51%, 33/64) showed saturating RLFs, i.e. they reached a maxR that did not increase any further with rising SPL (Fig. 4A). Forty-five percent of the units (29/64) had monotonic RLFs, i.e. firing rate increased steadily as a function of SPL (Fig. 4B). Only ~3% of the units (2/64) had non-monotonic RLFs, i.e. they showed an increase in firing rate as a function of SPL followed by a significant reduction in firing rate. This reduction was indicative of a second dynamic range at SPLs above where maximum firing was observed (Fig. 4C, see also below).

Based on the RLFs, the dynamic range of a unit was defined as the intensity range that differed significantly both from the level evoking the maxR and from the level showing the minimum firing rate (Wilcoxon rank sum). The median dynamic range for all units was 30 dB (25th and 75th percentiles: 20 and 40 dB; extremes 10–50 dB). The whole unit population covered a dynamic range of ~100 dB (−2 to 105 dB SPL). The mean lower limit of the dynamic range was 25 (SD 15) dB SPL, ranging from −2 to 65 dB SPL, the mean upper limit was 55 (SD 19) dB SPL, ranging from 12 to 105 dB SPL. The dynamic ranges of units with monotonic RLFs were significantly greater than of units with saturating RLFs [median (25th and 75th percentiles): 40 (27 and 40) dB vs. 20 (20 and 30) dB; $P < 0.005$, Wilcoxon rank sum]. In 2/64 units the firing rate decreased significantly after reaching a maximum, resulting in a second dynamic range at SPLs above the level of maximum firing.

Responses to SAM stimulation

General features and VS

In 54 units the responses to SAM stimuli were analysed with signals presented at CF to the contralateral ear. The SAM stimulation caused

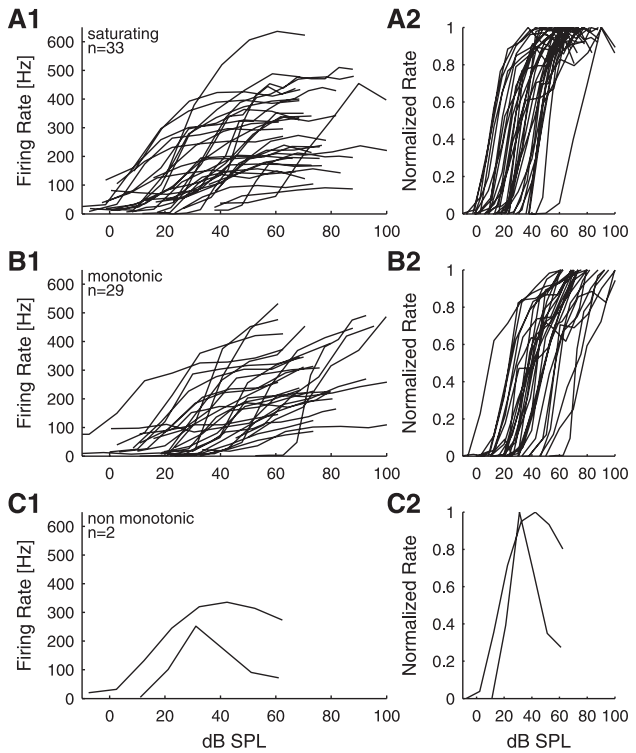

FIG. 4. RLFs (left) and normalized RLFs (right). (A) Saturating RLFs were observed in 33/64 units. (B) Twenty-nine units had monotonic RLFs. (C) Non-monotonic RLFs were found in 2/64 units. Right column: RLFs normalized to the units' spontaneous rates and their maxR.

periodically modulated responses, with the period length matching the period length of the modulation frequency (f_{AM}) in the stimulus (Fig. 5A).

Basing the quantification of responses to SAM stimuli on VS values, units showed low-pass modulation transfer functions (MTFs) at 10 (± 2) dB above threshold (Fig. 5B, 41 units tested at 10 ± 2 dB above threshold). The median MTF (VS-MTF) changed only slightly up to f_{AM} = 300 Hz. At values of f_{AM} > 300 Hz, VS values steadily decreased and typically fell below the VS value of the stimulus (VS = 0.5) at about 700 Hz. At f_{AM} = 1000 Hz, 88% of units (36/41) had VS values = 0.5. At even higher values of f_{AM}, in all units the VS values fell below 0.5.

VS values for responses to SAM stimulation are considerably lower than VS values calculated from responses to pure tone stimulations (Fig. 6). Units showed maximum synchronisation to pure tone stimulation at frequencies between 500 and 1500 Hz, with mean VS values of 0.7 (SD 0.1) and decreasing VS values at higher frequencies.

The majority of units did not show a selectivity for f_{AM} in their average firing rate. Their rate-based MTFs were mainly flat (Fig. 5C, same units as in Fig. 5B), indicating that at the level of the MNTB encoding of amplitude modulations relies on synchronous responses for temporal coding rather than on rate coding as seen at higher levels of the auditory pathway (Frisina, 2001; Joris *et al.*, 2004).

To analyse possible correlations with the characteristics of a unit's VS-MTF, the 3-dB cut-off frequency was calculated for the units' best VS-MTF, i.e. the VS-MTF of each unit showing the highest VS values. Cut-off frequencies varied between 370 and 1250 Hz, with the mean cut-off at 750 Hz (SD 200 Hz). Cut-off frequencies were correlated to the best f_{AM} (Spearman rank order correlation: 0.362, $P < 0.05$), but not to the maximum VS values ($P > 0.05$). The cut-off frequencies showed a significant increase with increasing CF (Spearman rank order correlation: 0.369, $P < 0.05$; Fig. 5D). If only units with CFs = 10 kHz were considered (as done for responses of auditory nerve fibres; Joris & Yin, 1992), the Spearman rank order correlation increased to 0.48 ($P < 0.05$). Cut-off values of units with CF > 10 kHz did not show a significant correlation with CF ($P > 0.05$). Tests failed to show correlations between cut-off frequency and other pure tone response properties, such as spontaneous activity, maximum rate, bandwidth and dynamic range (data not shown).

Influence of stimulus intensity on VS-MTFs

In 42 units SAM stimuli (100% modulation depth) were presented at different above-threshold levels. The overall trend in these units was a change from a low-pass VS-MTF to a band-pass VS-MTF as sound intensity increased, i.e. as the distance between the unit's response threshold and the peak intensity of the SAM stimulus increased (Fig. 7A). Additionally, maximum VS values of SAM stimuli presented at intensities close to threshold were higher than VS values of SAM stimuli presented at higher intensities (Spearman correlation coefficient: 0.644, $P < 0.05$; Fig. 7B).

Influence of modulation depth on responses to SAM stimuli

In 40 units SAM stimuli were presented at different modulation depths: 100, 75, 50 and 25%. To compare envelope synchronisation across modulation depths the modulation gain was calculated. Like the VS-MTFs of units, MTFs based on gain values had a low-pass shape (Fig. 7C). For all modulation depths median gain values were positive for values of f_{AM} up to 600 Hz, indicating a higher modulation depth in the response than in the stimulus. The lower the modulation depth the higher were the gain values. Gain values for 25 and 50% modulated SAM stimuli differed significantly from 100% modulated stimuli ($P < 0.05$, Mann–Whitney rank sum test).

Response latency

Response latencies were determined for 54 units using a reverse correlation method on the units' responses to SAM stimulation with values of f_{AM} between 595 and 1570 Hz (see Materials and methods). Latencies varied between 3 and 5.4 ms, with the mean at 4.4 ms. The higher a unit's CF the shorter was its latency (Fig. 5E; $P = 0.006$, Spearman correlation coefficient: −0.369).

Relationship between response properties and location in the MNTB

The reconstructions of the units' locations are based on the units' recording coordinates and the location of small electrolytic lesions set through the recording electrode at the end of the recording sessions (see Materials and methods for details; Fig. 8). In six animals we were able to analyse the relation between units' recording sites and the response properties both to unmodulated and modulated stimuli. In each animal the units' medio-lateral positions were related to the most medial recording track, which yielded acoustically excitable prepotential units, i.e. the physiological indicator of the medial border of the MNTB. Further, in each animal only units of recording tracks at the same medio-lateral plane were included in the analysis of medio-lateral gradients. To explore dorso-ventral gradients the recording depths of the units were set relative to the unit located most dorsally in the respective recording track. Two animals were excluded from this analysis because of the low number of single units.

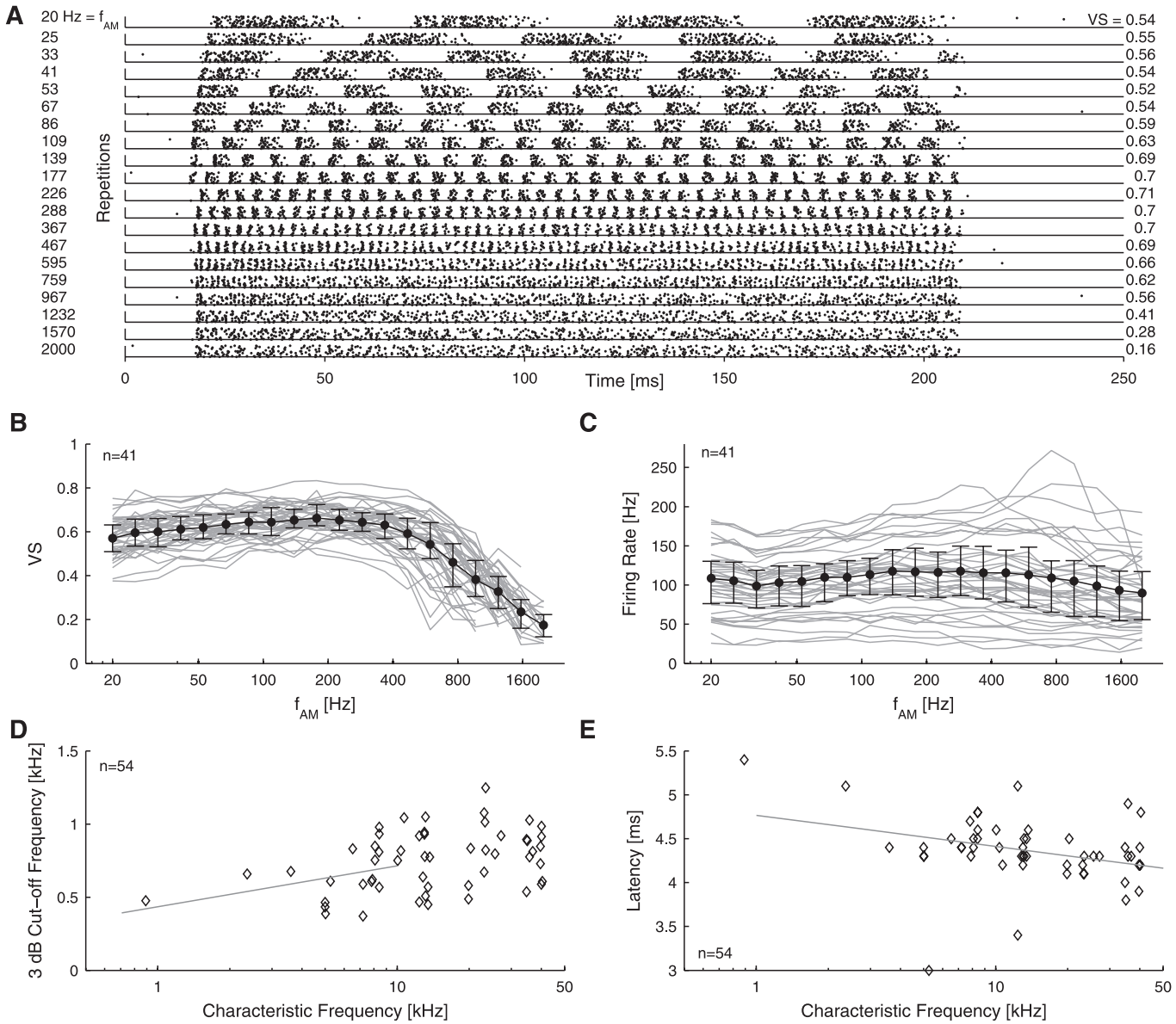

FIG. 5. Responses to SAM. (A) Dot raster displays of a unit (172-01) in response to SAM stimuli at the unit's characteristic frequency (CF; 35 kHz and 20 dB above threshold: 61 dB SPL). Stimulus length 200 ms; stimulus onset at 10 ms; 20 stimulus repetitions per f_{AM}; 100% modulation depth. The recordings showed periodically modulated firing rates, with the period length of the response matching the period length of the stimulus' modulation frequency (f_{AM} 20–2000 Hz, left column). Vector strength (VS) values are shown on the right. (B) Individual (grey) and median VS-based MTFs (VS-MTF, black, 25th and 75th percentiles) of 41 units display a low-pass shape [SAM stimulus: carrier frequency CF; stimulus level 10 (±2) dB above threshold; modulation depth 100%]. (C) Individual (grey) and median rate-based MTF (black, 25th and 75th percentiles, same units as in B) are mainly flat lacking pronounced peaks. (D) Cut-off frequency (3 dB) increases with increasing CF up to 10 kHz (Spearman rank order correlation: 0.48, $P < 0.05$). (E) Response latencies acquired from responses to SAM stimuli with a reverse correlation method show a dependence on CFs of units: the higher a unit's CF the shorter is its latency ($P = 0.006$, Spearman correlation coefficient: −0.369).

Medio-lateral axis

Based on the units acquired from animals in which recordings were made at more than one medio-lateral electrode position, tests were performed to identify possible gradients of response properties along the medio-lateral axis (Fig. 9). The analysis of CF along the respective axis showed a prominent tonotopic organisation (45 units, 15 tracks, five animals). Units with high CFs were located in the medial part of the MNTB, while units located progressively more lateral showed lower CFs. This observation holds true for all animals tested (Fig. 9A). The mean correlation coefficient r^2 was 0.66. Accordingly, response latencies increased along the medio-lateral axis, i.e. units located in the medial part of the MNTB had shorter response latencies than units situated further laterally. A respective correlation was observed in all animals tested (Fig. 9B, mean $r^2 = 0.34$). Same as for the CFs, in 4/5 animals the Q_{10} values tended to be high in units close to the medial nuclear border and showed a decrease to more lateral positions. Another response property with a trend for a medio-lateral gradient was the cut-off frequency of SAM responses, which also decreased for more lateral positions (Fig. 9C, mean $r^2 = 0.53$). The population analysis gave clear evidence that the latter three response properties were dependent on units' CFs. The other response properties, which

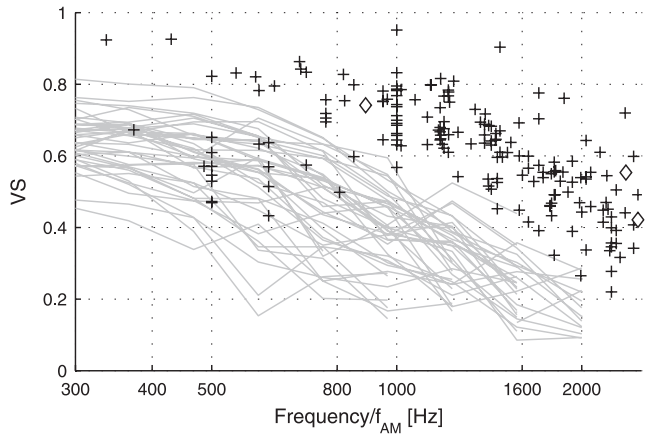

FIG. 6. Vector strength (VS) values for responses to pure tone stimulation (black crosses and diamonds, $n = 180$ from 24 units) and to SAM stimuli (grey lines, $n = 41$ units). Three of the units analysed for phase-locking to the stimulus period (diamonds) had their CF in the frequency range tested; for all other units VS values are calculated from responses to pure tones in the low-frequency tails of the units' FRAs. Note that the VS-MTF calculated for the f_{AM} range 300–2000 Hz (grey lines) typically cover lower ranges.

showed no systematic variation with CF, also did not show a clear topographic organisation medio-laterally.

Dorso-ventral axis

The analysis of possible dorso-ventral gradients of response properties is based on 43 units (11 tracks, six animals). The tonotopic organisation observed along the dorso-ventral axis was more ambiguous among animals than that observed along the medio-lateral axis. In 3/6 animals, units with higher CFs were located more ventrally (28 units in seven penetrations), but in the other three animals units with lower CFs were also found ventrally (15 units in four penetrations), suggesting that the fibrodendritic laminae in the MNTB are tilted in the sagittal plane. In contrast to the observations along the medio-lateral axis, CF-dependent response properties (response latency, Q_{10}, cut-off frequency) did not follow a clear trend along the dorso-ventral axis; not even if only animals showing the same dorso-ventral CF gradient were considered. MaxR was an exception. In all animals, units recorded from the more ventral parts of the MNTB had higher maxR values than units recorded more dorsally (Fig. 9D; mean $r^2 = 0.31$). We did not observe any correlation of location in the MNTB with either spontaneous rate or onset rate.

Discussion

The present study describes the response properties of MNTB units to pure tone pulses and amplitude-modulated stimuli, and demonstrates that these response properties vary with the anatomical location of the units in the MNTB. There are only a few reports of *in vivo* recordings in the MNTB of rat, and the primary question in these studies often concerns signal processing in targeting nuclei, rather than a detailed analysis of the response properties of the MNTB neurons (Sommer *et al.*, 1993; Kulesza *et al.*, 2003; Kadner *et al.*, 2006). In other species MNTB neurons are well characterised by *in vivo* preparations (cat: Tsuchitani, 1997; Joris & Yin, 1998; Smith *et al.*, 1998; mouse: Kopp-Scheinpflug *et al.*, 2003a; gerbil: Kopp-Scheinpflug *et al.*, 2003b). Though these studies give a good

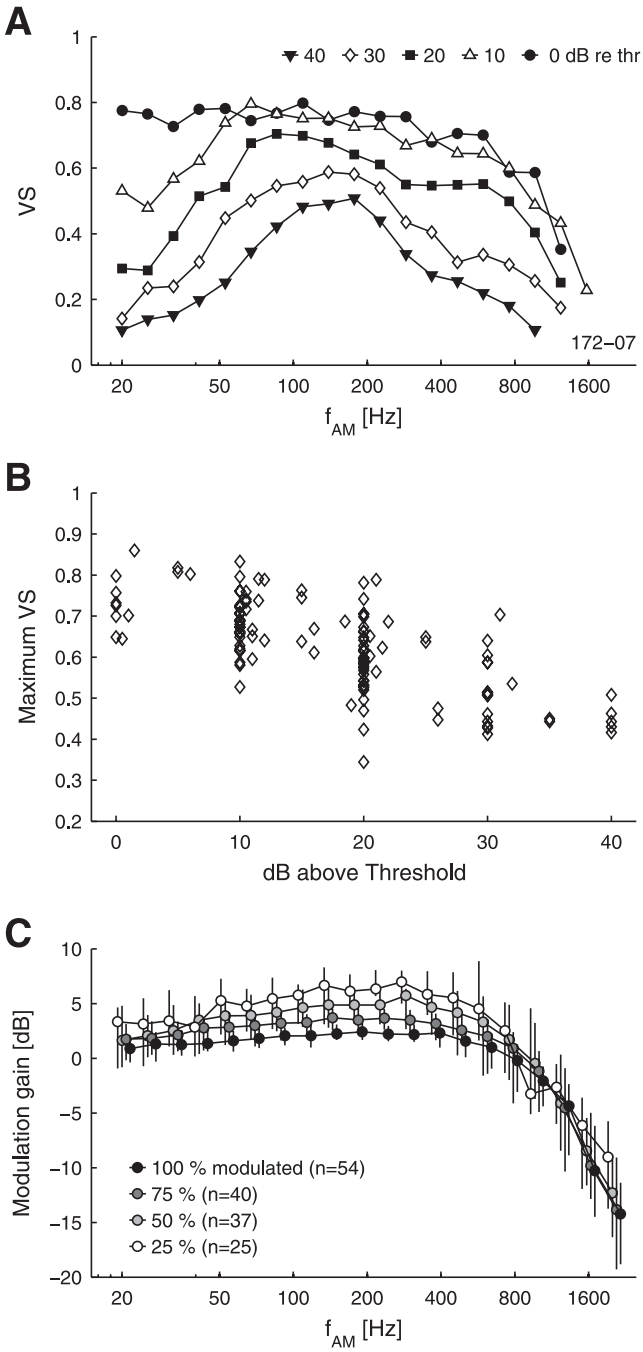

FIG. 7. Changes of vector strength (VS) with different stimulus levels and modulation gain with different modulation depths. (A) VS-MTF of unit 172-07 at 0 (filled circle), 10 (open triangle, peak up), 20 (filled square), 30 (open diamond) and 40 (black triangle, peak down) dB above threshold (CF: 20.3 kHz; threshold: 21 dB SPL). (B) Maximum VS values of units for different levels above threshold decrease with sound level increasing above threshold (Spearman correlation coefficient −0.644, $P < 0.05$). (C) Median MTFs based on modulation gain for different modulation depths. Modulation gain is greater for SAM stimuli of lower modulation depth. Irrespective of the modulation depth, gain values are positive for values of $f_{AM} < 600$ Hz.

insight into the general function of the MNTB in the auditory brainstem circuitry, they are hardly suited for an immediate comparison with rat *in vitro* data, one of the main model systems for studies of excitatory synaptic transmission in mammals (Schneggenburger & Forsythe, 2006).

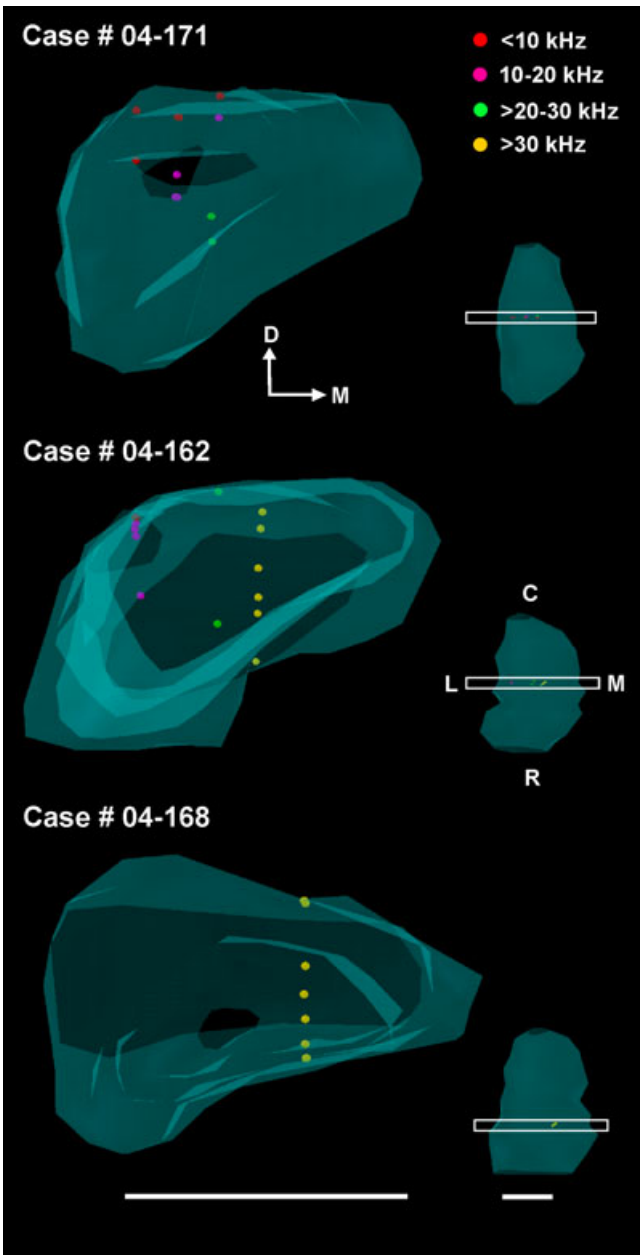

FIG. 8. Computer-assisted 3-d resonstructions of the left MNTB in three cases illustrating frequency distribution in a frontal-transverse view (color-coded on line, grey coded in print) Corresponding insets on the right show the rostro-caudal locations on horizontal views of the MNTB and recording tracks of these three cases. Note that neurons with high CFs are located medially, while units with low CFs are located progressively more laterally. Scale bars, 500 μm. C, caudal; M. medial; L, lateral; R, rostral; D, dorsal.

Our results show that MNTB units had V-shaped FRAs with and without low-frequency tail, and mostly saturating and non-saturating RLFs. PSTHs were mostly characterised as primary-like with notch or primary-like types. Units showed good phase-locking to SAM signals, and low-pass MTFs near threshold. The analysis of the location of the units demonstrates a topographic organisation along the medio-lateral axis for CF-dependent response properties, such as response latency, Q_{10} value and 3 dB cut-off-frequency, and a dorso-ventral gradient for the maxR, a CF-independent response feature.

Responses to pure tone pulses

Spectral properties

All but two units in our study had V-shaped FRAs in part with distinct low-frequency tails. These FRA shapes, already found in auditory nerve fibres (Kiang *et al.*, 1967, 1976; Sachs & Abbas, 1974; Schmiedt, 1989; el Barbary, 1991b), were described previously for MNTB neurons in cat (Tsuchitani, 1997) and gerbil (Kopp-Scheinpflug *et al.*, 2003b). More complex FRA types such as closed, high- or low-tilted, multi-peaked or narrow FRAs were not observed. Such response properties are found in nuclei that show a strong inhibitory input (AI: Sutter & Schreiner, 1991; IC: LeBeau *et al.*, 2001; AVCN: Kopp-Scheinpflug *et al.*, 2002; IC: Hernandez *et al.*, 2005; DNLL: Davis *et al.*, 2007). This suggests that unlike in these nuclei, systemic inhibitory input might only play a minor role in modulating the FRA shapes of MNTB units. Still, morphological studies showed that MNTB neurons are targeted by inhibitory inputs that are thought to originate from collaterals of MNTB efferents (Kuwabara & Zook, 1991; Kuwabara *et al.*, 1991; Smith *et al.*, 1991; Banks & Smith, 1992). However, the small percentage of non-monotonic FRAs and non-monotonic RLF suggests only weak acoustically evoked inhibitory input. Along the same lines, inhibitory sidebands, also ascribed to the influence of inhibitory inputs (Kopp-Scheinpflug *et al.*, 2006), were only found in a fraction of units.

Temporal response types

The vast majority of units showed phasic-tonic responses, with the most abundant PSTH types being primary-like with notch and primary-like patterns. The primary-like with notch pattern relates the MNTB cells to globular bushy cells, which were reported to have the same temporal response characteristics (Smith & Rhode, 1987; Smith *et al.*, 1991). This resemblance in the PSTH is also an indication of a fast 1 : 1 synaptic transmission at the calyx of Held. Yet, primary-like, phase-locked and even tonic responses were described previously for MNTB units as well (Tsuchitani, 1997; Smith *et al.*, 1998; Paolini *et al.*, 2001; Kopp-Scheinpflug *et al.*, 2003a,b; Kulesza *et al.*, 2003), suggesting different temporal dynamics of synaptic transmission *in vivo*.

Spontaneous activity

The median spontaneous activity of the units was 18 Hz (mean 29, SD 33), which is less than the mean spontaneous activity observed in earlier studies in rat (Sommer *et al.*, 1993; : 109 Hz; Kulesza *et al.*, 2003; : 46 Hz). The respective data from other species is more in the range of what we report here: 21 and ∼25 Hz in gerbil (Kopp-Scheinpflug *et al.*, 2003b; Hermann *et al.*, 2007) and 27 Hz in the cat (Smith *et al.*, 1998). Also, the number of units showing low to medium spontaneous activity corresponds to the present data [our study: <20 Hz, 53%; cat: <18 Hz, 55% (Smith *et al.*, 1998); <10 Hz, 67% (Tsuchitani, 1997); gerbil: <20 Hz, 72% (Hermann *et al.*, 2007)]. Again, the earlier studies in rats report lower numbers of units lacking spontaneous activity; these differences might be due to the use of different anaesthetic agents (present study: urethane; Kulesza *et al.*, 2003 : ketamine-xylazine; Sommer *et al.*, 1993 : ketamine-xylazine-chlorpromazine). Astl *et al.* (1996) showed that the number of spontaneously active IC neurons was higher in ketamine-xylazine- than in urethane- or pentobarbital-anaesthetized animals. More studies are needed for a conclusive clarification whether spontaneous activity in rat MNTB units indeed differs from other species.

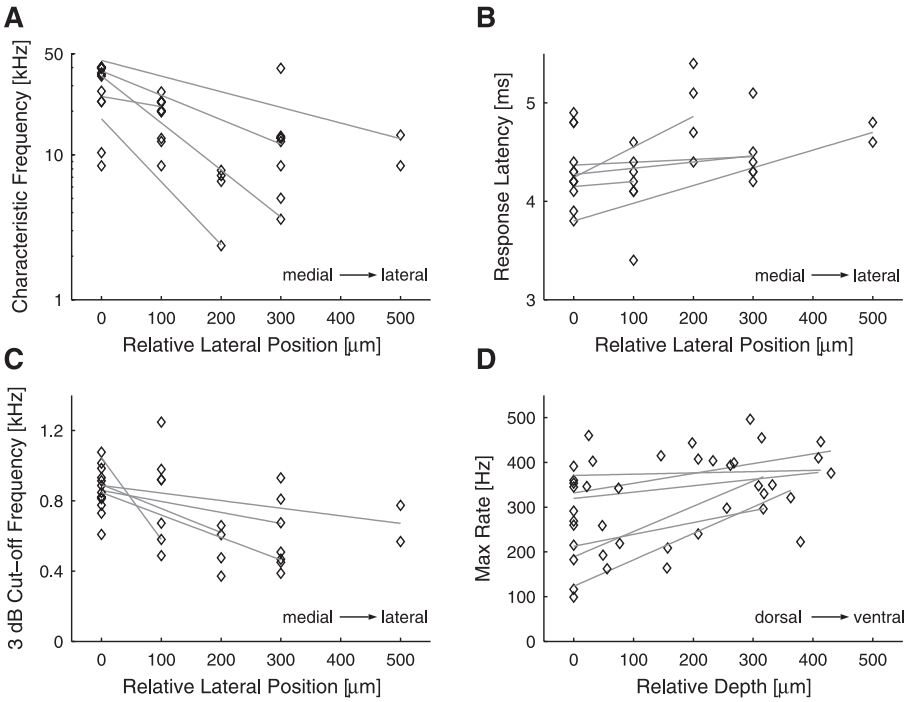

FIG. 9. Correlations between response properties and units' medio-lateral (A–C) and dorso-ventral positions (D). Graphs show case-specific correlations. (A) CF decreases with more lateral positions of units as does the 3 dB cut-off frequency (C). Response latency increases with more lateral positions (B). (D) MaxR increases towards more ventral positions of units.

Responses to modulated pure tones

Responses to amplitude-modulated stimuli in the MNTB were investigated in great detail in cat (Joris & Yin, 1998), while only a few studies addressed this question in rodent species (mouse: Kopp-Scheinpflug *et al.*, 2003a; gerbil: Tolnai *et al.*, 2006; rat: Kadner & Berrebi, 2008). Here we show that MNTB units in rat have low-pass MTFs. Cut-off frequencies are in the same range as in cat and exhibit the same tendency to increase with increasing CF (Joris & Yin, 1998). As a function of SPL we also observed phenomena like decreasing VS values (Joris & Yin, 1998) and a shift from low-pass- to band-pass-shaped MTFs as observed in other nuclei (Rees & Palmer, 1989; Frisina *et al.*, 1990; Kuwada & Batra, 1999; Krishna & Semple, 2000). Comparing SAM responses of MNTB units with those of globular bushy cells yields qualitatively similar results (Frisina *et al.*, 1990; Rhode & Greenberg, 1994; Joris & Yin, 1998). Due to the limited database, it is hard to estimate to which extent responses of MNTB units simply reflect the discharge characteristics of globular bushy cells or whether inhibition effectively shapes acoustically evoked MNTB signalling, as suggested by Kopp-Scheinpflug *et al.* (2003b).

In all species tested, the MNTB provides a precisely timed glycinergic inhibition to nuclei of the auditory brainstem encoding rapid transient shifts of stimulus levels. This is regarded as a prerequisite for the processing of azimuthal positions based on complex-structured high-frequency acoustic stimuli (Tollin, 2003) or encoding sound duration by units of the rat SPN (Kadner *et al.*, 2006). Recently it was shown that glycinergic projections from the MNTB to the SPN seem to be critical in generating off-responses in rat SPN units (Kulesza *et al.*, 2007). That way, phase-locked responses of MNTB units to AM stimuli would result in phase-locked responses in these units. And indeed, SPN units in rat show temporally modulated responses to SAM stimuli (Kulesza *et al.*, 2003), though the f_{AM} range to which SPN units phase-lock is smaller than the range in MNTB units (≤400 Hz vs. ≤700 Hz), which might be due to a slower time course of inhibitory inputs.

Topographic organisation and response properties

In the present study we showed that units' response properties are related to their medio-lateral and dorso-ventral position within the MNTB. Not unexpected, the strongest correlation between position and response property of a unit was observed for CF with a medial-to-lateral high-to-low frequency gradient. A comparable tonotopic organisation was shown in various species (cat: Guinan *et al.*, 1972b; cat: Smith *et al.*, 1991; rat: Sommer *et al.*, 1993; gerbil: Kopp-Scheinpflug *et al.*, 2003b), but it is still not clear to what extent the whole auditory range of a respective species finds a representation in the MNTB. In the present study we were able to directly show that response properties that were dependent on CF followed a medio-lateral gradient as well. These were the units' response latencies, Q_{10} values and SAM cut-off frequencies. A finding that needs to be explored in more detail was the correlation of the maxR (a CF-independent response property) with the dorso-ventral position of a unit. The more ventral a unit was located, the higher its maxR was.

The MNTB seems not to be a homogeneous nucleus as one might expect from its role in the circuitry encoding interaural intensity differences (for review see Yin, 2002 and Tollin, 2003). Though the functional significance is not entirely clear, our data add to reports that show gradients in MNTB cell properties such as a gradient observed in the size of MNTB somata (Guinan *et al.*, 1972a; Pasic *et al.*, 1994), an asymmetric distribution of ion channel subunits (Li *et al.*, 2001; Elezgarai *et al.*, 2003; von Hehn *et al.*, 2004), a non-uniform calbindin-labelling (Bazwinsky *et al.*, 2005) or a gradient in the phosphorylation of ion channel subunits (Song *et al.*, 2005). In

summary, these results suggest that the distinct physiological characteristics of MNTB principal cells should be taken into account when interpreting data obtained *in vitro*, and that our data, obtained in an undisturbed neuronal system, might thus serve as a basis for a connecting analysis of *in vitro* and *in vivo* data.

Acknowledgements

Financial support was provided by the Spanish MEC (BFU2006-00572) and JCYL (SA 007C05) to M.S.M., and the DFG to R.R. (Ru 390-18/1). S.T. and B.E. were supported by the Graduate Program INTERNEURO (GRK 1097) at the University of Leipzig, and O.H.G. by a postdoctoral contract (BFU2006-00572). A preliminary report was presented in the form of an abstract (Tolnai *et al.*, 2005).

Abbreviations

CF, characteristic frequency; FRA, frequency response area; IS, inverse slope; maxR, maximum firing rate; MNTB, medial nucleus of the trapezoid body; MTF, modulation transfer function; PSTH, post-stimulus time histogram; RLF, rate level function; SAM, sinusoidally amplitude-modulated; SPN, superior paraolivary nucleus; VS, vector strength.

References

Aoki, E., Semba, R., Keino, H., Kato, K. & Kashiwamata, S. (1988) Glycine-like immunoreactivity in the rat auditory pathway. *Brain Res.*, **442**, 63–71.

Astl, J., Popelar, J., Kvasnak, E. & Syka, J. (1996) Comparison of response properties of neurons in the inferior colliculus of guinea pigs under different anesthetics. *Audiology*, **35**, 335–345.

Banks, M.I. & Smith, P.H. (1992) Intracellular recordings from neurobiotin-labeled cells in brain slices of the rat medial nucleus of the trapezoid body. *J. Neurosci.*, **12**, 2819–2837.

el Barbary, A. (1991a) Auditory nerve of the normal and jaundiced rat. I. Spontaneous discharge rate and cochlear nerve histology. *Hear. Res.*, **54**, 75–90.

el Barbary, A. (1991b) Auditory nerve of the normal and jaundiced rat. II. Frequency selectivity and two-tone rate suppression. *Hear. Res.*, **54**, 91–104.

Barnes-Davies, M. & Forsythe, I.D. (1995) Pre- and postsynaptic glutamate receptors at a giant excitatory synapse in rat auditory brainstem slices. *J. Physiol. (Lond.)*, **488**, 387–406.

Bazwinsky, I., Bidmon, H.J., Zilles, K. & Hilbig, H. (2005) Characterization of the rhesus monkey superior olivary complex by calcium binding proteins and synaptophysin. *J. Anat.*, **207**, 745–761.

Borst, J.G., Helmchen, F. & Sakmann, B. (1995) Pre- and postsynaptic whole-cell recordings in the medial nucleus of the trapezoid body of the rat. *J. Physiol. (Lond.)*, **489**, 825–840.

Calford, M.B., Webster, W.R. & Semple, M.M. (1983) Measurement of frequency selectivity of single neurons in the central auditory pathway. *Hear. Res.*, **11**, 395–401.

Chuhma, N. & Ohmori, H. (1998) Postnatal development of phase-locked high-fidelity synaptic transmission in the medial nucleus of the trapezoid body of the rat. *J. Neurosci.*, **18**, 512–520.

Davis, K.A., Lomakin, O. & Pesavento, M.J. (2007) Response properties of single units in the dorsal nucleus of the lateral lemniscus of decerebrate cats. *J. Neurophysiol.*, **98**, 1475–1488.

Elezgarai, I., Diez, J., Puente, N., Azkue, J.J., Benitez, R., Bilbao, A., Knopfel, T., Donate-Oliver, F. & Grandes, P. (2003) Subcellular localization of the voltage-dependent potassium channel Kv3.1b in postnatal and adult rat medial nucleus of the trapezoid body. *Neuroscience*, **118**, 889–898.

Forsythe, I.D. (1994) Direct patch recording from identified presynaptic terminals mediating glutamatergic EPSCs in the rat CNS, in vitro. *J. Physiol.*, **479** (Pt. 3), 381–387.

Frisina, R.D. (2001) Subcortical neural coding mechanisms for auditory temporal processing. *Hear. Res.*, **158**, 1–27.

Frisina, R.D., Smith, R.L. & Chamberlain, S.C. (1990) Encoding of amplitude modulation in the gerbil cochlear nucleus: I. A hierarchy of enhancement. *Hear. Res.*, **44**, 99–122.

Futai, K., Okada, M., Matsuyama, K. & Takahashi, T. (2001) High-fidelity transmission acquired via a developmental decrease in NMDA receptor expression at an auditory synapse. *J. Neurosci.*, **21**, 3342–3349.

Goldberg, J.M. & Brown, P.B. (1969) Response of binaural neurons of dog superior olivary complex to dichotic tonal stimuli: some physiological mechanisms of sound localization. *J. Neurophysiol.*, **32**, 613–636.

Grandes, P. & Streit, P. (1989) Glutamate-like immunoreactivity in calyces of Held. *J. Neurocytol.*, **18**, 685–693.

Guinan, J.J.. Jr & Li, R.Y. (1990) Signal processing in brainstem auditory neurons which receive giant endings (calyces of Held) in the medial nucleus of the trapezoid body of the cat. *Hear. Res.*, **49**, 321–334.

Guinan, J.J.. Jr, Guinan, S.S. & Norris, B.E. (1972a) Single auditory units in the superior olivary complex I: responses to sounds and classification based on physiological properties. *Int. J. Neurosci.*, **4**, 101–120.

Guinan, J.J.. Jr, Norris, B.E. & Guinan, S.S. (1972b) Single auditory units in the superior olivary complex II: locations of unit categories and tonotopic organization. *Int. J. Neurosci.*, **4**, 147–166.

Harrison, J.M. & Warr, W.B. (1962) A study of the cochlear nuclei and ascending auditory pathways of the medulla. *J. Comp. Neurol.*, **119**, 341–379.

Heffner, H.E., Heffner, R.S., Contos, C. & Ott, T. (1994) Audiogram of the hooded Norway rat. *Hear. Res.*, **73**, 244–247.

von Hehn, C.A., Bhattacharjee, A. & Kaczmarek, L.K. (2004) Loss of Kv3.1 tonotopicity and alterations in cAMP response element-binding protein signaling in central auditory neurons of hearing impaired mice. *J. Neurosci.*, **24**, 1936–1940.

Held, H. (1893). Die zentrale Gehorleitung. In His, W. & Du Bois-Reymond, E. (Eds), *Archiv fur Anatomie und Physiologie*. Leipzig Verlag von Veit und Comp, Leipzig, pp. 201–380.

Hermann, J., Pecka, M., von Gersdorff, H., Grothe, B. & Klug, A. (2007) Synaptic transmission at the calyx of Held under in vivo like activity levels. *J. Neurophysiol.*, **98**, 807–820.

Hernandez, O., Espinosa, N., Perez-Gonzalez, D. & Malmierca, M.S. (2005) The inferior colliculus of the rat: a quantitative analysis of monaural frequency response areas. *Neuroscience*, **132**, 203–217.

Joris, P.X. & Yin, T.C. (1992) Responses to amplitude-modulated tones in the auditory nerve of the cat. *J. Acoust. Soc. Am.*, **91**, 215–232.

Joris, P.X. & Yin, T.C.T. (1998) Envelope coding in the lateral superior olive. III. Comparison with afferent pathways. *J. Neurophysiol.*, **79**, 253–269.

Joris, P.X., Schreiner, C.E. & Rees, A. (2004) Neural processing of amplitude-modulated sounds. *Physiol. Rev.*, **84**, 541–577.

Kadner, A. & Berrebi, A.S. (2008) Encoding of temporal features of auditory stimuli in the medial nucleus of the trapezoid body and superior paraolivary nucleus of the rat. *Neuroscience*, **151**, 868–887.

Kadner, A., Kulesza, R.J. Jr & Berrebi, A.S. (2006) Neurons in the medial nucleus of the trapezoid body and superior paraolivary nucleus of the rat may play a role in sound duration coding. *J. Neurophysiol.*, **95**, 1499–1508.

Kiang, N.Y., Sachs, M.B. & Peake, W.T. (1967) Shapes of tuning curves for single auditory-nerve fibers. *J. Acoust. Soc. Am.*, **42**, 1341–1342.

Kiang, N.Y., Liberman, M.C. & Levine, R.A. (1976) Auditory-nerve activity in cats exposed to ototoxic drugs and high-intensity sounds. *Ann. Otol. Rhinol. Laryngol.*, **85**, 752–768.

Kopp-Scheinpflug, C., Dehmel, S., Dorrscheidt, G.J. & Rubsamen, R. (2002) Interaction of excitation and inhibition in anteroventral cochlear nucleus neurons that receive large endbulb synaptic endings. *J. Neurosci.*, **22**, 11004–11018.

Kopp-Scheinpflug, C., Fuchs, K., Lippe, W.R., Tempel, B.L. & Rubsamen, R. (2003a) Decreased temporal precision of auditory signaling in Kcna1-null mice: an electrophysiological study in vivo. *J. Neurosci.*, **23**, 9199–9207.

Kopp-Scheinpflug, C., Lippe, W.R., Dorrscheidt, G.J. & Rubsamen, R. (2003b) The medial nucleus of the trapezoid body in the gerbil is more than a relay: comparison of pre- and postsynaptic activity. *J. Assoc. Res. Otolaryngol.*, **4**, 1–23.

Kopp-Scheinpflug, C., Dehmel, S. & Rubsamen, R. (2006) *Opposite Actions of Glycine at a Mammalian Central Synapse*. Midwinter Meeting of the Association for Research in Otolaryngology, Abstract no. 679, Baltimore, MD.

Krishna, B.S. & Semple, M.N. (2000) Auditory temporal processing: responses to sinusoidally amplitude-modulated tones in the inferior colliculus. *J. Neurophysiol.*, **84**, 255–273.

Kulesza, R.J. Jr, Spirou, G.A. & Berrebi, A.S. (2003) Physiological response properties of neurons in the superior paraolivary nucleus of the rat. *J. Neurophysiol.*, **89**, 2299–2312.

Kulesza, R.J. Jr, Kadner, A. & Berrebi, A.S. (2007) Distinct roles for glycine and GABA in shaping the response properties of neurons in the superior paraolivary nucleus of the rat. *J. Neurophysiol.*, **97**, 1610–1620.

Kuwabara, N. & Zook, J.M. (1991) Classification of the principal cells of the medial nucleus of the trapezoid body. *J. Comp. Neurol.*, **314**, 707–720.

Kuwabara, N., DiCaprio, R.A. & Zook, J.M. (1991) Afferents to the medial nucleus of the trapezoid body and their collateral projections. *J. Comp. Neurol.*, **314**, 684–706.

Kuwada, S. & Batra, R. (1999) Coding of sound envelopes by inhibitory rebound in neurons of the superior olivary complex in the unanesthetized rabbit. *J. Neurosci.*, **19**, 2273–2287.

LeBeau, F.E., Malmierca, M.S. & Rees, A. (2001) Iontophoresis in vivo demonstrates a key role for GABA(A) and glycinergic inhibition in shaping frequency response areas in the inferior colliculus of guinea pig. *J. Neurosci.*, **21**, 7303–7312.

Li, W., Kaczmarek, L.K. & Perney, T.M. (2001) Localization of two high-threshold potassium channel subunits in the rat central auditory system. *J. Comp. Neurol.*, **437**, 196–218.

Liberman, M.C. (1978) Auditory-nerve response from cats raised in a low-noise chamber. *J. Acoust. Soc. Am.*, **63**, 442–455.

Malmierca, M.S. (2003) The structure and physiology of the rat auditory system: an overview. *Int. Rev. Neurobiol.*, **56**, 147–211.

Merrill, E.G. & Ainsworth, A. (1972) Glass-coated platinum-plated tungsten microelectrodes. *Med. Biol. Eng.*, **10**, 662–672.

Moore, M.J. & Caspary, D.M. (1983) Strychnine blocks binaural inhibition in lateral superior olivary neurons. *J. Neurosci.*, **3**, 237–242.

Morest, D.K. (1968) The growth of synaptic endings in the mammalian brain: a study of the calyces of the trapezoid body. *Z. Anat. Entwicklungsgesch.*, **127**, 201–220.

Paolini, A.G., FitzGerald, J.V., Burkitt, A.N. & Clark, G.M. (2001) Temporal processing from the auditory nerve to the medial nucleus of the trapezoid body in the rat. *Hear. Res.*, **159**, 101–116.

Pasic, T.R., Moore, D.R. & Rubel, E.W. (1994) Effect of altered neuronal activity on cell size in the medial nucleus of the trapezoid body and ventral cochlear nucleus of the gerbil. *J. Comp. Neurol.*, **348**, 111–120.

Rees, A. & Palmer, A.R. (1989) Neuronal responses to amplitude-modulated and pure-tone stimuli in the guinea pig inferior colliculus, and their modification by broadband noise. *J. Acoust. Soc. Am.*, **85**, 1978–1994.

Rhode, W.S. & Greenberg, S. (1994) Encoding of amplitude modulation in the cochlear nucleus of the cat. *J. Neurophysiol.*, **71**, 1797–1825.

Sachs, M.B. & Abbas, P.J. (1974) Rate versus level functions for auditory-nerve fibers in cats: tone-burst stimuli. *J. Acoust. Soc. Am.*, **56**, 1835–1847.

Schmiedt, R.A. (1989) Spontaneous rates, thresholds and tuning of auditory-nerve fibers in the gerbil: comparisons to cat data. *Hear. Res.*, **42**, 23–35.

Schneggenburger, R. & Forsythe, I.D. (2006) The calyx of Held. *Cell Tissue Res.*, **326**, 311–337.

Smith, P.H. & Rhode, W.S. (1987) Characterization of HRP-labeled globular bushy cells in the cat anteroventral cochlear nucleus. *J. Comp. Neurol.*, **266**, 360–375.

Smith, P.H., Joris, P.X., Carney, L.H. & Yin, T.C. (1991) Projections of physiologically characterized globular bushy cell axons from the cochlear nucleus of the cat. *J. Comp. Neurol.*, **304**, 387–407.

Smith, P.H., Joris, P.X. & Yin, T.C. (1998) Anatomy and physiology of principal cells of the medial nucleus of the trapezoid body (MNTB) of the cat. *J. Neurophysiol.*, **79**, 3127–3142.

Sommer, I., Lingenhohl, K. & Friauf, E. (1993) Principal cells of the rat medial nucleus of the trapezoid body: an intracellular in vivo study of their physiology and morphology. *Exp. Brain Res.*, **95**, 223–239.

Song, P., Yang, Y., Barnes-Davies, M., Bhattacharjee, A., Hamann, M., Forsythe, I.D., Oliver, D.L. & Kaczmarek, L.K. (2005) Acoustic environment determines phosphorylation state of the Kv3.1 potassium channel in auditory neurons. *Nat. Neurosci.*, **8**, 1335–1342.

Spangler, K.M., Warr, W.B. & Henkel, C.K. (1985) The projections of principal cells of the medial nucleus of the trapezoid body in the cat. *J. Comp. Neurol.*, **238**, 249–262.

Spirou, G.A., Brownell, W.E. & Zidanic, M. (1990) Recordings from cat trapezoid body and HRP labeling of globular bushy cell axons. *J. Neurophysiol.*, **63**, 1169–1190.

Sutter, M.L. (2000) Shapes and level tolerances of frequency tuning curves in primary auditory cortex: quantitative measures and population codes. *J. Neurophysiol.*, **84**, 1012–1025.

Sutter, M.L. & Schreiner, C.E. (1991) Physiology and topography of neurons with multipeaked tuning curves in cat primary auditory cortex. *J. Neurophysiol.*, **65**, 1207–1226.

Taschenberger, H. & von Gersdorff, H. (2000) Fine-tuning an auditory synapse for speed and fidelity: developmental changes in presynaptic waveform, EPSC kinetics, and synaptic plasticity. *J. Neurosci.*, **20**, 9162–9173.

Tolbert, L.P., Morest, D.K. & Yurgelun-Todd, D.A. (1982) The neuronal architecture of the anteroventral cochlear nucleus of the cat in the region of the cochlear nerve root: horseradish peroxidase labelling of identified cell types. *Neuroscience*, **7**, 3031–3052.

Tollin, D.J. (2003) The lateral superior olive: a functional role in sound source localization. *Neuroscientist*, **9**, 127–143.

Tollin, D.J. & Yin, T.C. (2005) Interaural phase and level difference sensitivity in low-frequency neurons in the lateral superior olive. *J. Neurosci.*, **25**, 10648–10657.

Tolnai, S., Hernandez, O., Rubsamen, R. & Malmierca, M.S. (2005) *The Medial Nucleus of the Trapezoid Body: An In Vivo Electrophysiological Study in Rat*. Midwinter Meeting of the Association for Research in Otolaryngology, New Orleans, LA.

Tolnai, S., Englitz, B., Dehmel, S., Kopp-Scheinpflug, C., Jost, J. & Rübsamen, R. (2006) *Temporal Properties of Inhibition shaping the Response of MNTB Principal Cells*. Midwinter Meeting of the Association for Research in Otolaryngology, Denver, CO.

Tsuchitani, C. (1997) Input from the medial nucleus of trapezoid body to an interaural level detector. *Hear. Res.*, **105**, 211–224.

Wenthold, R.J., Huie, D., Altschuler, R.A. & Reeks, K.A. (1987) Glycine immunoreactivity localized in the cochlear nucleus and superior olivary complex. *Neuroscience*, **22**, 897–912.

Yin, T.C.T. 2002. Neural mechanisms of encoding binaural localization cues in the auditory brainstem. In Oertel, D., Popper, A.N. & Fay, R.R. (Eds), *Integrative Functions in the Mammalian Auditory Pathway*. Springer-Verlag, New York, pp. 99–159.